Molecular Neurobiology (2019) 56:6261–6275
https://doi.org/10.1007/s12035-019-1515-4

Changes in Dendritic Spine Density and Inhibitory Perisomatic Connectivity onto Medium Spiny Neurons in L-Dopa-Induced Dyskinesia

G. Gomez[1,2] · M. V. Escande[3] · L. M. Suarez[4,5] · L. Rela[3] · J. E. Belforte[3] · R. Moratalla[4,5] · M. G. Murer[3] · O. S. Gershanik[1,2] · I. R. E. Taravini[1,2,6]

Received: 8 November 2018 / Accepted: 28 January 2019 / Published online: 11 February 2019
© Springer Science+Business Media, LLC, part of Springer Nature 2019

Abstract

Using bacterial artificial chromosome–double transgenic mice expressing tdTomato in D1 receptor-medium spiny neurons (MSNs) and enhanced green fluorescent protein in D2 receptor-MSNs, we have studied changes in spine density and perisomatic GABAergic boutons density in MSNs of both the D1R and D2R pathways, in an experimental model of parkinsonism (mouse injected with 6-hydroxydopamine in the medial forebrain bundle), both in the parkinsonian and dyskinetic condition induced by L-DOPA treatment. To assess changes in perisomatic GABAergic connectivity onto MSNs, we measured the number of contacts originated from parvalbumin (PV)-containing striatal "fast-spiking" interneurons (FSIs), the major component of a feed-forward inhibition mechanism that regulates spike timing in MSNs, in both cell types as well as the number of vesicular GABA transporter (VGAT) contacts. Furthermore, we determined changes in PV-immunoreactive cell density by PV immunolabeling combined with *Wisteria floribunda* agglutinin (WFA) labeling to detect FSI in a PV-independent manner. We also explored the differential expression of striatal activity–regulated cytoskeleton-associated protein (Arc) and c-Fos in both types of MSNs as a measure of neuronal activation. Our results confirm previous findings of major structural changes in dendritic spine density after nigrostriatal denervation, which are further modified in the dyskinetic condition. Moreover, the finding of differential modifications in perisomatic GABAergic connectivity and neuronal activation in MSNs suggests an attempt by the system to regain homeostasis after denervation and an imbalance between excitation and inhibition leading to the development of dyskinesia after exposure to L-DOPA.

Keywords Parkinson's disease · L-DOPA-induced dyskinesia · Medium spiny neuron · Dendritic spines · Parvalbumin

Electronic supplementary material The online version of this article (https://doi.org/10.1007/s12035-019-1515-4) contains supplementary material, which is available to authorized users.

✉ I. R. E. Taravini
irenetaravini@gmail.com

1 Facultad de Farmacia y Bioquímica, Universidad de Buenos Aires, Ciudad Autónoma de Buenos Aires, Argentina

2 Instituto de Investigaciones Farmacológicas (ININFA), Laboratorio de Parkinson Experimental, CONICET - Universidad de Buenos Aires, Ciudad Autónoma de Buenos Aires, Argentina

3 Instituto de Fisiología y Biofísica (IFIBIO) Bernardo Houssay, Grupo de Neurociencia de Sistemas, Universidad de Buenos Aires, CONICET, Buenos Aires, Argentina

4 Instituto Cajal, Consejo Superior de Investigaciones Científicas (CSIC), Madrid, Spain

5 CIBERNED, Instituto de Salud Carlos III, Madrid, Spain

6 Laboratorio de Neurobiología Experimental (LNE), CONICET - Facultad de Bromatología, Universidad Nacional de Entre Ríos, Gualeguaychú, Entre Ríos, Argentina

Introduction

The dopamine (DA) precursor L-DOPA has been the gold standard pharmacological treatment of Parkinson's disease (PD) for the past 50 years [1]. However, a significant number of patients develop motor complications including abnormal involuntary movements (AIM) termed L-DOPA-induced dyskinesia (LID), during chronic L-DOPA therapy. Several studies show the occurrence of structural plastic changes in the striatum of parkinsonian animals in association with the development of LID, but there are still unresolved issues regarding how L-DOPA modifies striatal connectivity.

Neuroplasticity can be defined as the ability of the nervous system to respond to intrinsic or extrinsic stimuli by reorganizing its structure, function, and connections [2]. While these processes are associated with many physiological phenomena such as learning and memory [3], under certain conditions, they can become detrimental. A disturbance of the system could trigger modifications in an attempt to restore its

normal functioning, but the persistence and lack of reversibility of such modifications may turn them maladaptive. Structural plasticity comprises anatomical changes in synapse numbers, spine density, axonal and dendritic branching patterns, synaptic connectivity patterns, and even neuronal cell numbers [4]. The balance between the number of inhibitory and excitatory synapses is one form of network plasticity [5–8].

Striatal medium spiny neurons (MSNs) are organized in two GABAergic projection systems. The neurons of the direct pathway selectively express the DA D1 receptors (D1R-MSNs) [9, 10], while the MSNs of the indirect pathway express the DA D2 receptors (D2R-MSNs) [11, 12]. MSNs have a large dendritic tree densely covered by dendritic spines. Glutamatergic and dopaminergic afferents converge over MSN dendrites to regulate basal ganglia–mediated movement and cognition functions [12]. Spines are considered the smallest anatomical structure where the biochemical and electrophysiological signals of the glutamatergic and dopaminergic synapses are integrated [13]. Thus, spine density modifications induced by a nigrostriatal lesion and L-DOPA therapy have been a topic of increasing interest during the past decade. In a previous work, we showed that striatal DA depletion induces a reduction of dendritic spine density in both types of MSNs which is exclusively reversed by a chronic L-DOPA treatment in the MSNs of the indirect pathway [14, 15]. In contrast, studies from other laboratories have found spine depletion in D1R-MSNs only after chronic L-DOPA treatment but not after 6-OHDA injection [16, 17]. The discordant findings could be related to differences in experimental approaches, including the different animal models used by different groups (e.g., nigrostriatal lesions induced by toxin injections at the striatum or medial forebrain bundle) [14, 16–18].

Inhibition of MSNs comes from axon collaterals of neighboring MSNs and from striatal GABAergic interneurons [19, 20]. Despite their low number, striatal interneurons critically modulate corticostriatal synaptic plasticity and MSN excitability, and therefore influence striatal output. In particular, parvalbumin-immunoreactive (PV-ir) striatal interneurons, also known as fast-spiking interneurons (FSIs), are the major component of a feed-forward inhibition mechanism that regulates spike timing in MSNs [21], thus coordinating neuronal synchrony in the striatum [22]. FSI synapses are located proximally on each MSN [23] and tend to form pericellular baskets around the somata of both types of MSNs [10, 24–26]. Perisomatic inhibition is particularly efficient at silencing neuronal output because of its close proximity to the axon initial segment where spikes are generated [20]. Studies analyzing structural changes in the interaction between FSI and MSNs after DA depletion have reached opposite conclusions [27, 28] and their role in LID development has not yet been studied.

Overall, the different results obtained by different laboratories preclude drawing conclusions about how the number of excitatory and inhibitory connections over MSNs of the direct and indirect pathway changes after nigrostriatal lesions and chronic L-DOPA treatment. As an initial attempt to characterize this balance, we have studied changes in spine density and perisomatic GABAergic boutons density in MSNs of both pathways, in the same experimental model of parkinsonism (mouse injected with 6-OHDA in the medial forebrain bundle), both in the parkinsonian and dyskinetic condition.

Materials and Methods

Animals

The study was performed on adult female C57BL/6 wild-type mice and bacterial artificial chromosome in C57Bl6 (BAC)-double transgenic mice expressing tdTomato in D1R-MSNs [29] and enhanced green fluorescent protein (EGFP) in D2R-MSNs (The Jackson Laboratory, USA). The animals weighed 25–28 g at the beginning of the experiments and were caged in groups of five, in a temperature-controlled room (20 °C ± 2 °C), with a 12:12-h light/dark cycle and ad libitum access to food pellets and tap water. The surgical procedure and experimental treatments were performed in accordance with European Council Directive 2010/63/EU guidelines for the care of laboratory animals and the regulations for the Care and Use of Laboratory Animals of the National Institutes of Health, USA. Animal experiments were approved by our local Ethics Committee (IACUC EXP-UBA No. 0027665/2014). The animals were anesthetized with inhalatory isoflurane before the surgical procedure.

Drugs

Isofluorane 100% (Nicholas Piramal (I) Ltd, UK), bupivacain hydrochloride (5 mg/ml, AstraZeneca, Argentina), 6-hydroxydopamine hydrobromide (6-OHDA, Sigma, USA), ascorbic acid (Sigma, USA), L-3,4-dihidroxiphenyl-alanine methyl ester hydrochloride (L-DOPA, Sigma, USA) and benserazide hydrochloride (Sigma, USA), sterile glucose-saline solution (5%, Rivero, Argentina).

Unilateral 6-OHDA Lesion

Under deep inhalatory anesthesia (isofluorane 4% in O_2 for 2 min for induction and 2% for maintenance), mice received a stereotaxic injection of 6-OHDA (2 μg as freebase/0.5 μl/min) in the left medial forebrain bundle, so as to produce a severe degeneration of the nigrostriatal pathway, or vehicle (0.02% ascorbic acid in saline) [30]. Stereotaxic coordinates used 1.0 mm posterior, 1.1 mm lateral from bregma, and 4.8 mm ventral from dura [31]. For control groups (SHAM), a simulated lesion was performed by injection of the same volume of

vehicle at the same coordinates. After surgery, the analgesic bupivacaine hydrochloride (5 mg/ml) was injected subcutaneously (s.c.; 10 μl/10 g body weight) in two sites around the wound. To minimize mortality caused by the severe dopaminergic denervation, mice received intensive postoperative care. During the 3 weeks after surgery, mice received sterile glucose-saline solution (0.1 ml/10 g body weight, s.c.) twice a day to avoid dehydration. In addition, to complement food intake, animals received a commercially available nutritional supplement (Ensure® Plus, Argentina). This solution was administered per os using a plastic Pasteur pipette (1 ml, twice a day). This procedure allowed a 100% survival of lesioned animals after surgery.

Behavioral Evaluation of the 6-OHDA Lesion

Three weeks after surgery, selection of the successfully denervated animals was performed by testing akinesia of the contralateral paw with a limb use asymmetry test (cylinder test, CT) [32–34] which evaluates the forelimb use during spontaneous vertical exploration in a cylindrical enclosure. To perform this test, mice were put in a transparent acrylic cylinder (10 cm diameter, 20 cm height) and an observer counted the number of wall contacts performed independently with the left, the right, or both forepaws for 3 min or the time necessary to perform a total of 10 supporting wall contacts (one session only). No habituation of the animals to the cylinder was allowed before the testing session. An asymmetry of forelimb use score was calculated as the number of contralateral forepaw wall contacts plus one-half the number of both forelimbs' wall contacts, divided by the total number of wall contacts per session [35]. Animals with less than 20% of contralateral forepaw use were considered to be appropriately denervated and used for the experiments.

L-DOPA Treatment and Behavioral Evaluation

Four weeks after surgery, the 6-OHDA-lesioned animals were randomly separated in two groups and received a daily intraperitoneal injection of physiological saline as vehicle (6-OHDA/VEH group) or L-DOPA and the peripheral DOPA decarboxylase inhibitor benserazide (12/12 mg/kg respectively) dissolved in saline solution (6-OHDA/L-DOPA group) for 15 days. SHAM animals were treated with saline for 15 days (SHAM/VEH group). The drugs were dissolved immediately prior to use and injected at the volume of 0.1 ml/10 g body weight.

The abnormal involuntary movements or dyskinesias were measured after L-DOPA (or VEH) administration on days 1, 4, 8, and 12 every 20 min over a period of 180 min in each session. Each measure was performed for 1 min by a blinded observer. The AIM were classified into three different subtypes: forelimb dyskinesia (FD), axial dystonia (AD), and orofacial dyskinesia (OD), and scored on a severity scale that goes from 0 to 4 (0: absent; 1: occasional; 2: frequent; 3: continuous interrupted by sensory distraction; 4: continuous, severe, and not interrupted by sensory distraction) [32, 36–38]. Therefore, the sum of the three AIM in each observation every 20 min was between 0 and 12, while the sum of the maximum AIM was the sum of the maximum score obtained for each AIM subtype in each session.

Immunohistochemical Assay

At the end of the experiments, 1 h after the last L-DOPA (or VEH) injection, the animals were deeply anesthetized and transcardially perfused with cold paraformaldehyde 4% in 0.1 M phosphate buffer (PB). Brains were dissected out and post-fixed overnight (ON) in the same fixative solution at 4 °C.

Mice brains used for the evaluation of spine density were serially sectioned in a vibratome at the striatum level. Serial sections from the whole striatum were collected as follows: four 200-μm-thick tissue sections were taken intercalated by three 30-μm-thick tissue sections. Free-floating coronal 200-μm-thick tissue sections were used for Lucifer yellow (LY) injections of tdTomato-positive (two sections) or EGFP-positive MSNs (two sections), and alternate 30-μm-thick tissue sections were used for tyrosine hydroxylase (TH) and FosB immunohistochemistry and for PV and VGAT immunofluorescence [14, 15]. Twelve to 14 neurons per section were injected with LY, but only those appropriately labeled were considered for further analysis. An equal number of D2R- and D1R-MSNs was injected. BAC-double transgenic mice and wild-type mice used for immunofluorescent staining were serially sectioned in a freezing microtome and the free-floating coronal 30-μm-thick tissue sections were stored in PB 0.9% saline (PBS) containing 0.1% sodium azide at 4 °C.

Immunohistochemistry was performed on free-floating coronal sections following standard protocols [14, 39, 40]. During all staining procedures, 0.1 M PBS containing 0.3% Triton X-100 (PBS-T) was used for diluting all immunoreagents and for washing between all antibody incubations. The following primary antisera were used: rabbit anti-TH (1:1,000; PelFreez Biologicals, USA), rabbit anti-FosB (1:10,000; Santa Cruz Biotechnology, USA), rabbit anti-LY (1:100,000; [41]), mouse anti-PV (1:2,000; Swant, Switzerland), guinea pig anti-VGAT (vesicular GABA transporter, 1:500; Synaptic Systems, USA), rabbit anti-c-Fos (1:500; Santa Cruz Biotechnology, USA), rabbit anti-Arc (activity-regulated cytoskeleton-associated protein, 1:1,000; Synaptic system, Germany). In all immunostaining procedures, each primary antibody was once omitted from the experimental protocol to determine its specificity leading to no tissue labeling (not shown). For colorimetric immunolabeling,

the sections were incubated with the corresponding biotin-labeled antisera (1:250; Vector Laboratories, USA) and the presence of the primary antibody was visualized by means of an avidin-biotin peroxidase complex (1:125; Vectastain, ELITE ABC kit, Vector Laboratories, USA), developed with 0.5 mg/ml 3,3′-diaminobenzidine tetrahydrochloride (Sigma, USA) and 0.015% H_2O_2. For PV, VGAT, c-Fos, or Arc immunofluorescent staining was performed in BAC-double transgenic mice: two sections per animal were incubated separately with the antibodies described above and the following secondary antisera: goat anti-mouse Cy5 (1:500; Jackson Immunoresearch, USA) for PV and goat anti-rabbit Cy5 (1:500; Jackson Immunoresearch, USA) for c-Fos and Arc. VGAT was developed using goat anti-guinea pig biotinylated (1:250; Vector Laboratories, USA) and streptavidin-Cy5 (1:200; Jackson Immunoresearch, USA).

Perineuronal nets that can be detected by *Wisteria floribunda* agglutinin (WFA) labeling surround most FSI. WFA is a lectin that binds to carbohydrate moieties on proteoglycans that form perineuronal nets [42]. WFA appears to preferentially bind carbohydrate structures terminating in N-acetylgalactosamine linked α or β to the 3 or 6 position of galactose and has been used to detect FSI in a PV-independent manner [42]. PV immunolabeling combined with *Wisteria floribunda* agglutinin (WFA) labeling was performed on free-floating coronal sections of wild-type mice. Two tissue sections per animal were incubated ON at 4 °C in mouse anti-PV, followed by an ON incubation with biotin-labeled WFA (1:1,000; Vector Laboratories, USA). Each antigen was developed using goat anti-mouse Cy3 (1:500; Jackson Immunoresearch, USA) and streptavidin-Cy5 (1:200; Jackson Immunoresearch, USA), respectively.

Morphological Analysis and Spine Quantification

The autofluorescence of D1R-MSNs and D2R-MSNs were visualized using an E600FN Nikon microscope by means of specific filters for those fluorophores. In different 200-μm tissue sections, D1R-MSNs or D2R-MSNs were individually injected with LY following published protocols [14, 43]. After that, the injected cells were visualized by immunohistochemistry using the anti-LY antibody (as described before) [14]. Dendritic tree reconstruction of MSNs and spine quantification were performed under transmitted light at × 100 magnification using the software Mercator Pro (Explora Nova, France) [43]. Spine quantification of striatal D1R-MSNs and D2R-MSNs was expressed as the number of spines per 10 μm of dendritic length. Sholl analysis of the dendritic tree was performed using the National Institutes of Health (NIH, USA) ImageJ software running the Sholl Analysis Plugin. A grid with concentric rings distributed at equal distances (15 μm) was superimposed and centered in the soma of each neuron reconstruction [37]. The number of dendritic intersections per ring was computed and branching complexity, total dendritic length, and maximum dendritic span were evaluated [44].

Image Analysis and Quantification

Images of diaminobenzidine-immunolabeled sections were captured with a Nikon Eclipse 50i microscope equipped with a Nikon DS-5MCL1 cooled camera. The percentage of TH-immunoreactive (TH-ir) area was determined on both lesioned and unlesioned striata on every 12th 30-μm-thick coronal section (a total of six sections covering the striatum between 1.1 and − 0.4 mm related to bregma) [31, 40]. Optical density measurements were performed using the ImageJ software (NIH, USA).

Fluorescent images were acquired with an Olympus FV1000 confocal microscope (IFIBIO Houssay microscopy facility). For PV or VGAT perisomatic contact quantifications, six pictures per animal using × 60 optical zoom and × 2.5 digital zoom were taken from dorsolateral striatum of two different tissue sections. The number of PV or VGAT boutons onto each D1R-MSN or D2R-MSN was counted using ImageJ software and cell counter plugin (NIH, USA). For c-Fos and Arc expression, two pictures per animal using × 20 optical zoom were taken from dorsolateral striatum of two different tissue sections. The percentage of each MSN subtype in dorsolateral striatum co-expressing c-Fos or Arc was counted using the software ImageJ (NIH, USA). For PV and WFA co-localization, two photographs per animal, using × 20 optical zoom, were taken from dorsolateral striatum of two different tissue sections. The PV-ir and WFA-labeled cell densities in dorsolateral striatum were determined using the software ImageJ.

Statistical Analysis

Data analyses were performed using Graph Prism 4 Version 5.0. Statistical tests are described in each figure legend. Compiled data that passed the Shapiro-Wilks normality test was analyzed by means of one-way or two-way analysis of variance (ANOVA) or two-way repeated measures ANOVA followed, when significant differences existed, by the post hoc Bonferroni's or Newman-Keuls multiple comparison test and represented as mean ± SEM. PV and VGAT perisomatic boutons were analyzed using a one-way nested ANOVA followed by the post hoc Newman-Keuls multiple comparison test. Comparisons of data that did not fit a normal distribution were done with a Kruskal-Wallis ANOVA followed by the Dunn's multiple comparisons test, and were represented as median and ranges. In all tests, significance was assigned when $p < 0.05$.

Results

Dendritic and Spine Density Changes After 6-OHDA Lesion and L-DOPA-Induced Dyskinesia

In BAC D1R-tdTomato/D2R-EGFP double transgenic mice, unilateral 6-OHDA medial forebrain bundle injection induced an almost complete ipsilateral DA depletion, observed both by TH immunohistochemistry and by the cylinder test. Hemiparkinsonian mice treated daily with L-DOPA developed severe AIM (dyskinesias) in the contralateral forelimb, trunk, and orofacial musculature (see Supplementary Fig. 1). In fixed 200-μm-thick coronal striatal sections, tdTomato-positive and EGFP-positive neurons were injected with LY by microiontophoresis under direct visual observation. LY was then developed by immunohistochemistry with diaminobenzidine as chromogen, to allow the visualization of labeled neurons under bright-field illumination (Fig. 1(a_1–a_4)). We performed a Sholl analysis of dendritic tree on morphologically reconstructed striatal D1R-MSNs (Fig. 1(b_1)) and D2R-MSNs (Fig. 1(c_1)) in SHAM/VEH, 6-OHDA/VEH, and 6-OHDA/L-DOPA animals. A two-way ANOVA of repeated measures (experimental groups vs distance from soma) of number of intersections of D2R-MSNs revealed small but significant effects of lesion and treatment at specific distances from soma (interaction: $F_{(24,468)} = 2.02$, $p = 0.0032$; Fig. 1(c_2)), while no significant effects were found for the number of dendritic branching (Fig. 1(c_3)), or D1R-MSNs (Fig. 1(b_2, b_3)). Effects of cell type (D1R-MSN and D2R-MSN) and experimental condition on total Sholl intersections, total branching points, total dendritic length, and maximum dendritic span were assessed with additional two-way ANOVAs (Supplementary Fig. 2). Overall, D2R-MSNs showed a smaller number of intersections ($F_{(1,81)} = 4.35$; cell type effect, $p = 0.040$, Supplementary Fig. 2a) and a shorter dendritic span ($F_{(1,81)} = 21.43$; cell type effect, $p < 0.0001$, Supplementary Fig. 2d) compared with D1R-MSNs, regardless of the experimental group (nonsignificant effects of experimental condition and interaction). This is in agreement with previous findings by Fieblinger et al. [17]. Other dendritic parameters, like number of branching points or total length of the dendritic arbor, were not different between cell types (Supplementary Fig. 2b, c).

Spines were counted in the longest dendrite of each sampled D1R-MSN or D2R-MSN (Fig. 1d). In SHAM/VEH animals, there was no significant difference in the number of spines between D1R-MSNs and D2R-MSNs (6.87 ± 0.75 and 6.86 ± 0.57, spines per 10 μm, respectively). Our data show a similar and marked reduction of spines in both D1R-MSNs and D2R-MSNs after 6-OHDA injection (3.89 ± 0.40 and 4.27 ± 0.36, respectively) in agreement with previous results [14, 15, 45]. Moreover, chronic L-DOPA at doses inducing dyskinesia restored a normal spine density in the dendrites of D2R-MSNs but had no effect on D1R-MSNs (6.04 ± 0.28 and 3.67 ± 0.50). Cell type and treatment effects were assessed with a two-way ANOVA, which revealed significant effects of both factors ($F_{(1,76)} = 4.81$, $p = 0.031$ and $F_{(2,76)} = 16.03$, $p < 0.0001$, respectively) and a nonsignificant interaction ($p = 0.055$). Bonferroni post hoc tests showed that the D2R-MSNs from L-DOPA-treated animals have significantly more spines than the D2R-MSNs from 6-OHDA-lesioned vehicle-treated animals ($p < 0.05$) and do not differ from SHAM-lesioned mice D2R-MSNs. Moreover, D2R-MSNs have more spines than D1R-MSNs in the L-DOPA-treated animals ($p < 0.01$). Thus, the data show a depletion of spines in D1R- and D2R-MSNs after nigrostriatal denervation and a recovery of spine density to control levels in D2R-MSNs during a chronic L-DOPA treatment that was capable of inducing AIM. These results are in agreement with previous findings by Suárez et al. [14] obtained using similar methods but after local injection of 6-OHDA in the striatum in mice reporting either D1R- or D2R-MSN with fluorescent proteins.

Striatal Parvalbumin-Containing Interneurons and MSN Connectivity

The connectivity state between PV striatal interneurons and MSNs expressing either D1 or D2 receptors in the dyskinetic condition remains elusive. To answer this question, we assessed the number of perisomatic PV synaptic boutons onto D1R-MSNs and D2R-MSNs (Fig. 2a). One-way nested ANOVA revealed significant differences between experimental groups for both D1R- and D2R-MSNs ($F_{(2,154)} = 50.52$, $p < 0.0001$; $F_{(2,153)} = 40.80$, $p < 0.0001$; respectively).

In 6-OHDA-lesioned mice treated with VEH, we observed a reduction of PV contacts in both D1R-MSNs and D2R-MSNs compared with SHAM/VEH mice (D1R-MSNs 2.02 ± 0.19 vs 4.10 ± 0.30 contacts per cell, $p < 0.05$; D2R-MSNs 1.74 ± 0.20 vs 3.21 ± 0.28 contacts per cell, $p < 0.05$; Newman-Keuls post hoc test). A small but significant further decrease in PV-ir contacts was observed after L-DOPA administration in 6-OHDA mice for both types of MSNs (D1R-MSNs 1.19 ± 0.22, $p < 0.05$; D2R-MSNs 1.13 ± 0.18, $p < 0.05$; Newman-Keuls post hoc test) compared with 6-OHDA/VEH mice (Fig. 2b, c). Thus, the lesion decreased the number of perisomatic PV-ir contacts in both cell types and L-DOPA did not counteract the lesion effect.

Changes in the number of PV-ir boutons could be due to disappearance of the boutons or to reduced expression of PV in the boutons. To further understand the structural changes in perisomatic inhibition induced by the treatments, we looked at the number of perisomatic VGAT contacts (Fig. 2d, e). In control animals, the number of perisomatic VGAT-ir contacts was similar to that of PV-ir boutons both in D1R-MSNs and D2R-MSNs (VGAT-ir D1R-MSNs 3.85 ± 0.19 contacts per cell; D2R-MSNs 2.72 ± 0.23 contacts per cell), supporting

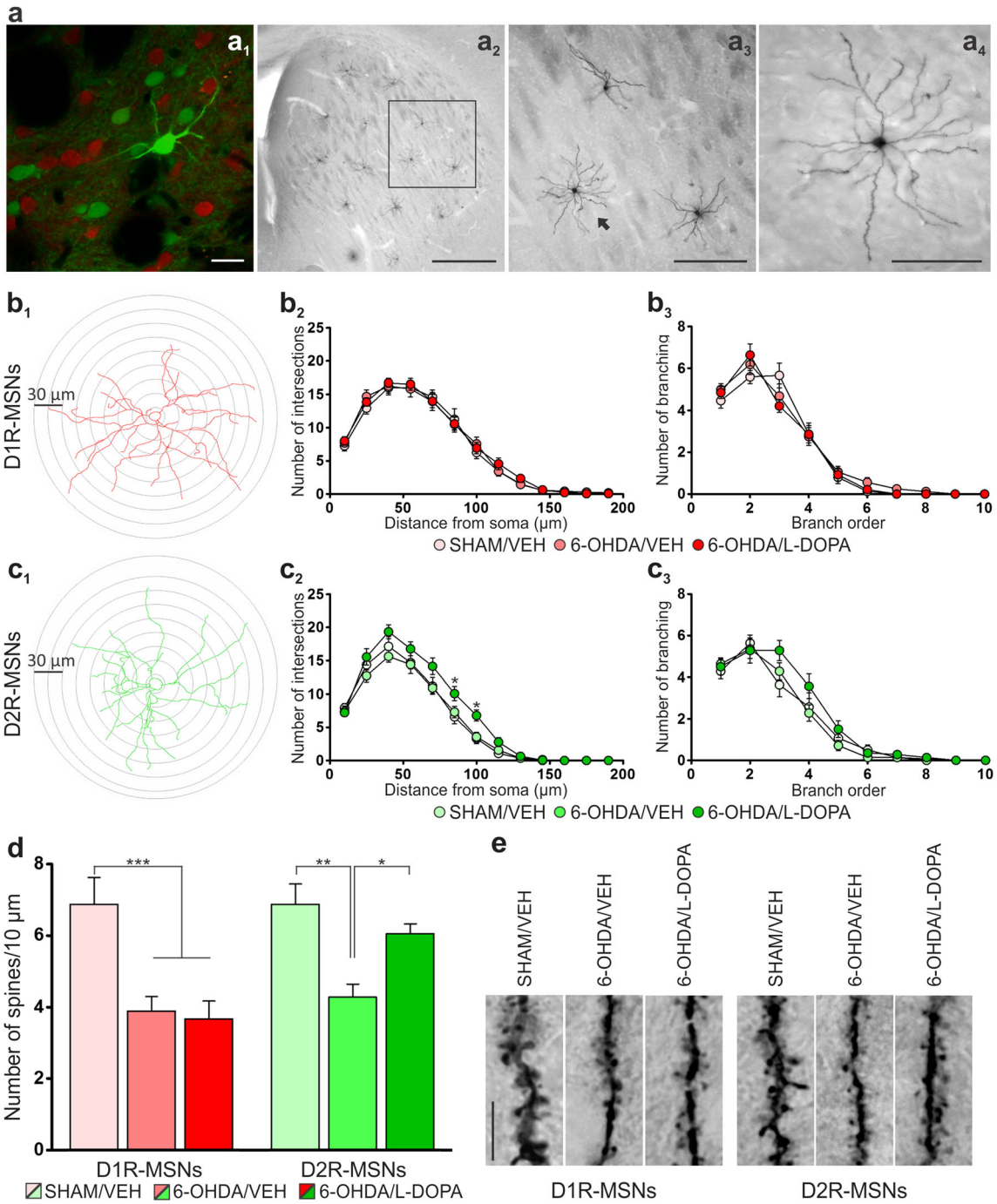

Fig. 1 **a** (a_1) Single MSN injected with Lucifer yellow in a 200-µm-thick striatal tissue section of a BAC-double transgenic mice. Scale bar: 20 µm. (a_2) Striatal section showing Lucifer yellow injected MSNs after diaminobenzidine immunostaining. Scale bar: 500 µm. (a_3) The arrow indicates the MSN showed at high magnification in figure (a_4). Scale bar: (a_3) 200 µm; (a_4) 100 µm. **b**, **c** Dendritic tree morphometric evaluation of the D1R-MSNs and D2R-MSNs by Sholl analysis. (b_1, c_1) Schematic representations of a D1R- and D2R-MSN, respectively. (b_2, b_3) Number of intersections and number of branching of the D1R-MSNs, respectively. (c_2, c_3) Number of intersections and number of branching of the D2R-MSNs, respectively. Statistical analysis: $*p < 0.05$; post hoc Bonferroni's multiple comparison test after significant interaction in two-way ANOVA with repeated measures only for number of intersections of D2R-MSNs (c_2) ($p = 0.0032$). **d** Spine quantification of striatal D1R-MSNs and D2R-MSNs under the different experimental conditions (mean ± SEM). Statistical analysis: $*p < 0.05$, $**p < 0.01$, $***p < 0.001$; post hoc Bonferroni's multiple comparison test after significant differences in in two-way ANOVA. **e** High magnification microphotographs showing a portion of dendrite from D1R-MSNs and D2R-MSNs under the different experimental conditions. Scale bar: 10 µm. SHAM/VEH, $n = 4$; 6-OHDA/VEH, $n = 5$; 6-OHDA/L-DOPA, $n = 4$

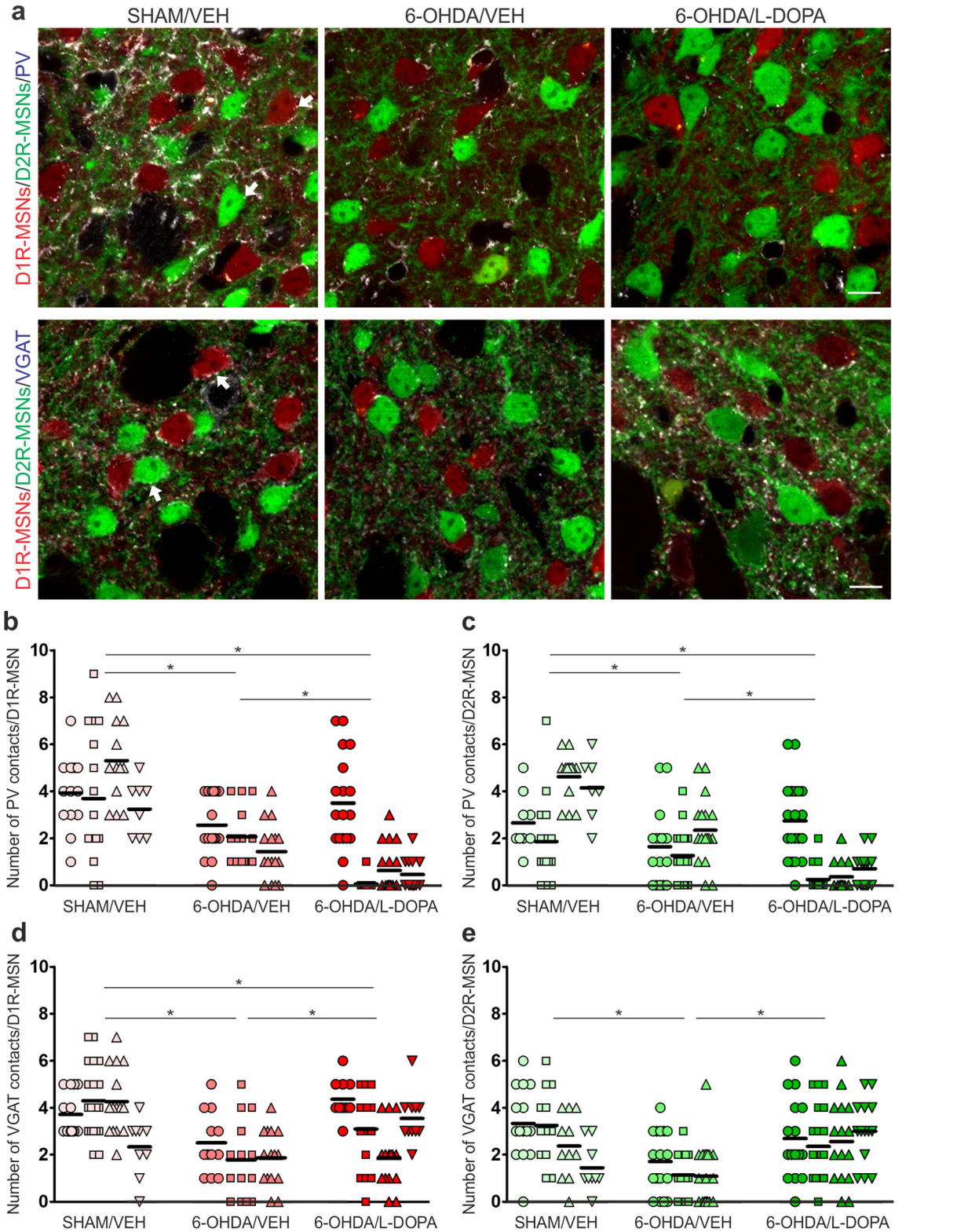

Fig. 2 **a** Confocal microphotographs of the dorsolateral striatum of double transgenic mice showing the autofluorescence of D1R-MSNs (red) and D2R-MSNs (green) and the immunofluorescence of PV or VGAT (white). The arrow heads indicate the perisomatic PV-ir synapses onto D1R- or D2R-MSNs. Scale bar: 10 μm. Quantification of perisomatic PV-ir boutons onto D1R-MSNs (**b**) or D2R-MSNs (**c**). Quantification of perisomatic VGAT-ir boutons onto D1R-MSNs (**d**) or D2R-MSNs (**e**). SHAM/VEH, $n = 4$; 6-OHDA/VEH, $n = 3$; 6-OHDA/L-DOPA, $n = 4$. *p 0.05; post hoc Newman-Keuls multiple comparison test after significant differences in one-way nested ANOVA

the view that perisomatic inhibition comes mainly from PV-ir neurons. One-way nested ANOVAs revealed significant effects of the treatments on VGAT-ir contacts for each cell type (D1R-MSNs: $F_{(2,147)} = 17.41$, $p < 0.0001$; D2R-MSNs: $F_{(2,148)} = 11.47$, $p = 0.000023$). The number of VGAT boutons was reduced after the 6-OHDA lesions in both types of MSNs (D1R-MSNs 2.02 ± 0.22, $p < 0.05$; D2R-MSNs 1.30 ± 0.17, $p < 0.05$; Newman-Keuls post hoc test), supporting a structural effect of the lesion rather than just a reduction of PV expression. Finally, chronic L-DOPA induced a recovery of perisomatic VGAT boutons for D2R-MSNs (2.62 ± 0.20; $p < 0.05$ vs 6-OHDA/VEH mice, $p = 0.87$ vs SHAM mice), and a partial recovery for D1R-MSNs (3.10 ± 0.20; $p < 0.05$ vs SHAM mice, $p < 0.05$ vs 6-OHDA/VEH mice). Together with the lack of recovery of PV contacts in L-DOPA-treated mice, these results suggest a structural remodeling of perisomatic inhibition in dyskinetic animals.

Parvalbumin-Containing Interneurons and *Wisteria floribunda* Agglutinin–Labeled Cells in Wild-type Mice

The lower levels of striatal PV-ir boutons found after 6-OHDA injection and after L-DOPA treatment could be explained by a loss of FSI and/or reduced levels of PV protein in the axon terminals of these interneurons. Some studies investigating PV cell density in related hyperkinetic disorders like Tourette syndrome, dystonia, and Huntington's disease have revealed a reduced number of FSI in these pathologic conditions [45–47], suggesting that they could also be affected in LID. Based on this assumption, we analyzed PV-ir cell density in the injected striatum by immunofluorescent labeling using a new group of wild-type mice with the same degree of DA depletion and similar results in terms of AIM development with either VEH or L-DOPA compared with the BAC transgenic mice (see Supplementary Fig. 3). On images taken with a confocal microscope, we quantified the number of PV-ir neurons. One-way ANOVA revealed a significant effect of treatment ($F_{(2,15)} = 4.88$, $p = 0.023$). We found that PV-ir cell density was reduced in both 6-OHDA experimental groups compared with SHAM mice (6-OHDA/VEH: $p < 0.05$; 6-OHDA/L-DOPA: $p < 0.05$), with no difference between these groups (SHAM/VEH, 28.85 ± 1.95 cells/mm^2; 6-OHDA/VEH, 19.71 ± 1.35 cells/mm^2; 6-OHDA/L-DOPA, 20.73 ± 3.12 cells/mm^2) (Fig. 3a).

To further confirm that reduced levels of PV-ir somata and axon terminals were not due to a reduction in PV expression but to a reduction in FSI number, we analyzed PV-ir cells as well as WFA-labeled cells by double fluorescence labeling. WFA labels extracellular matrix components around FSI (perineuronal nets). On images taken with a confocal microscope, we quantified WFA-labeled neurons that were also PV-ir (Fig. 3b). One-way ANOVA revealed a significant effect of treatment ($F_{(2,15)} = 4.24$, $p = 0.035$), which was explained by a significant decrease of WFA+/PV+ cells in 6-OHDA/VEH animals compared with sham animals (SHAM/VEH 20.76 ± 1.51 cells/mm^2; 6-OHDA/VEH 12.56 ± 1.67 cells/mm^2; $p < 0.05$, Newman-Keuls post hoc test). The 6-OHDA/L-DOPA animals had a WFA+/PV+ cell density which was half-way up to control levels, not differing significantly from any of the other two experimental groups (16.63 ± 2.58 cells/mm^2). Interestingly, co-localization of WFA labeling and PV immunolabeling showed that even in SHAM mice, there were some WFA-labeled cells that did not contain PV (SHAM/VEH 6.69 ± 2.01 cells/mm^2). Furthermore, the number of WFA-labeled cells that were not PV-ir was similar in the three experimental groups (SHAM/VEH 6.69 ± 2.01 cells/mm^2; 6-OHDA/VEH 8.62 ± 2.10 cells/mm^2; 6-OHDA/L-DOPA 6.77 ± 1.61 cells/mm^2; $p = 0.75$). Overall, the data show that the lesion reduces the number of PV-ir cells and particularly of those PV-ir cells surrounded by a WFA+ perineuronal nets, and suggest that even though L-DOPA administration does not produce a recovery of PV-ir cells, it partially restores the PV cells that have nets labeled with WFA, as their levels are not different from 6-OHDA/VEH, nor from SHAM/VEH (Fig. 3c).

Striatal Activity–Regulated Cytoskeleton-Associated Protein (Arc) and c-Fos Expression After L-DOPA Treatment

After completing the evaluation of the dendritic spine density and the perisomatic inhibitory inputs, we evaluated whether their impact on MSNs remains balanced after dopaminergic manipulation in both pathways by measuring the Arc and c-Fos as markers of the neuronal response to different stimuli.

Immunohistochemical assay for Arc showed no expression in SHAM or 6-OHDA mice treated with VEH. In contrast, Arc expression was evident only in the striatum of dyskinetic animals (6-OHDA mice treated with L-DOPA). The results showed expression of Arc (blue) in the cellular somata and dendrites of all D1R-MSNs (red) while the only D2R-MSNs (green) expressing Arc co-expressed the D1 receptor (Fig. 4a, Table 1).

Immunofluorescent analysis showed either very low or even absent nuclear c-Fos expression in the striatum of SHAM mice, whereas in the 6-OHDA/VEH group, there was an increase of c-Fos immunoreactivity only in D2R-MSNs. More specifically, none of the D1R-MSNs expressed c-Fos (less than 1%) and half of the D2R-MSNs were c-Fos-ir ($51 \pm 13\%$) in 6-OHDA/VEH animals. Notably, these D2R-MSNs did not co-express the D1 receptor. Moreover, after L-DOPA treatment, the expression of c-Fos was further increased and changed from one cell type to the other, showing an increased expression only in the D1R-MSNs ($99 \pm 1\%$) and in a few D2R-MSNs ($1 \pm 1\%$) which co-expressed the D1 receptor as seen in Arc immunodetection (Fig. 4b, Table 1).

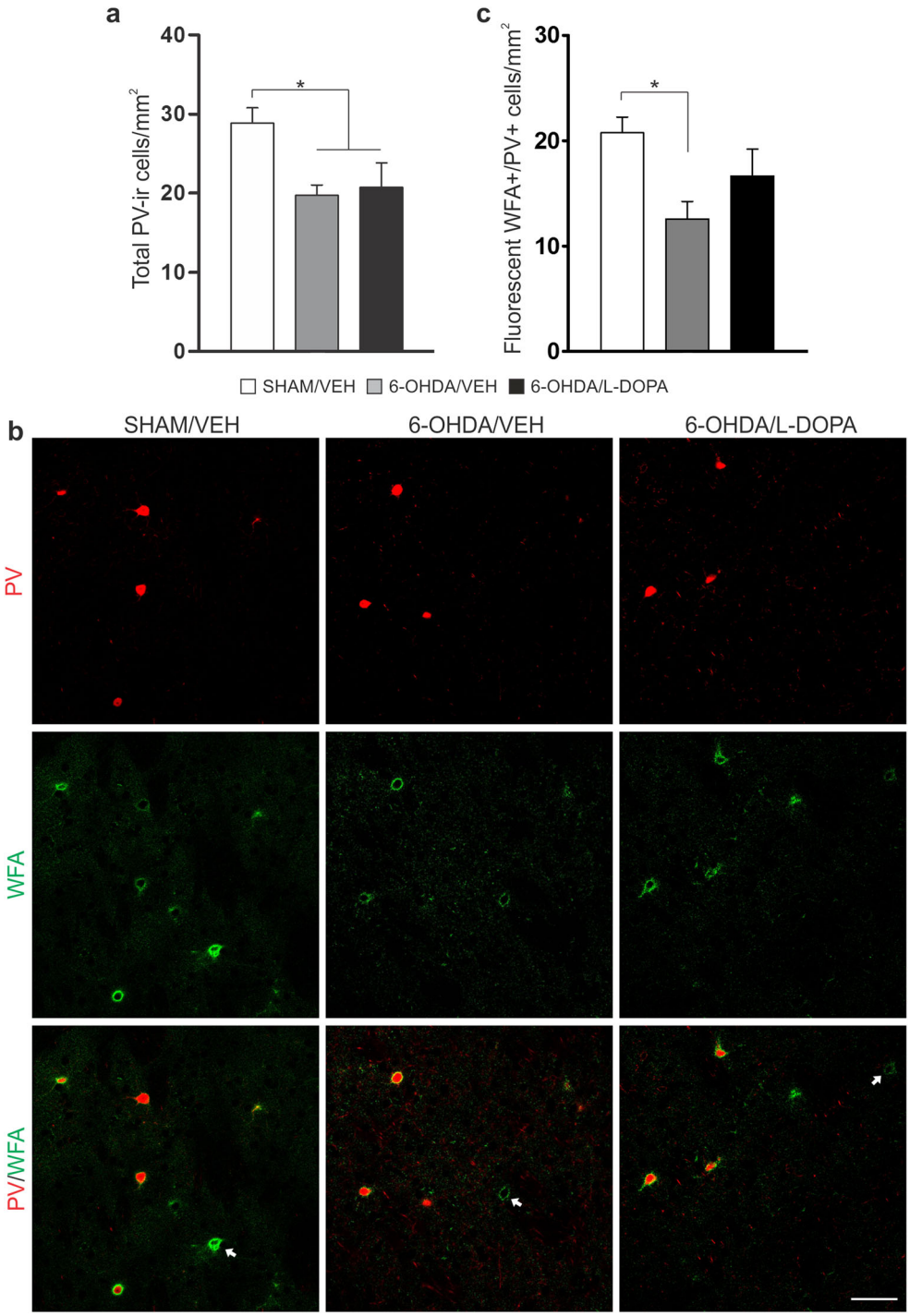

Fig. 3 **a** Density of PV-ir interneurons in the dorsolateral striatum under the different experimental conditions (mean± SEM). *$p < 0.05$; post hoc Newman-Keuls multiple comparison test after significant differences in one-way ANOVA test. **b** Representative confocal microphotograph of the dorsolateral striatum of wild-type mice showing the immunofluorescence of PV labeling (red) and WFA labeling (green). Arrows indicate WFA-labeled cells that did not contain PV in the three experimental groups. Scale bar: 50 μm. **c** Quantification of dorsolateral striatal WFA-labeled cells that present immunoreactivity for PV under the different experimental conditions (mean ± SEM). *$p < 0.05$; post hoc Newman-Keuls multiple comparison test after significant differences in one-way ANOVA test. SHAM/VEH, $n = 7$; 6-OHDA/VEH, $n = 5$; 6-OHDA/L-DOPA, $n = 6$

Discussion

Morphological plastic changes of MSNs dendrites were first found in the brain of PD patients [46, 47]. This gave rise to several studies using animal models of PD and LID aiming to describe the microstructural remodeling that takes place in the dendritic arbor and spines of MSNs. Even though there is a general consensus that spine pruning of the MSNs is strongly associated with the extent of the dopaminergic denervation, there are some discrepancies regarding the adaptations that differentially occur in the populations of MSNs [14, 16–18]. Here, we induced a severe dopaminergic denervation by injecting 6-OHDA into the medial forebrain bundle of double transgenic mice which enabled us to analyze the two populations of MSNs in the same animal. We showed that pruning occurs in both D1R- and D2R-MSNs after DA depletion and that there is a restoration of spine density in D2R-MSNs but not in D1R-MSNs after chronic L-DOPA administration, thus

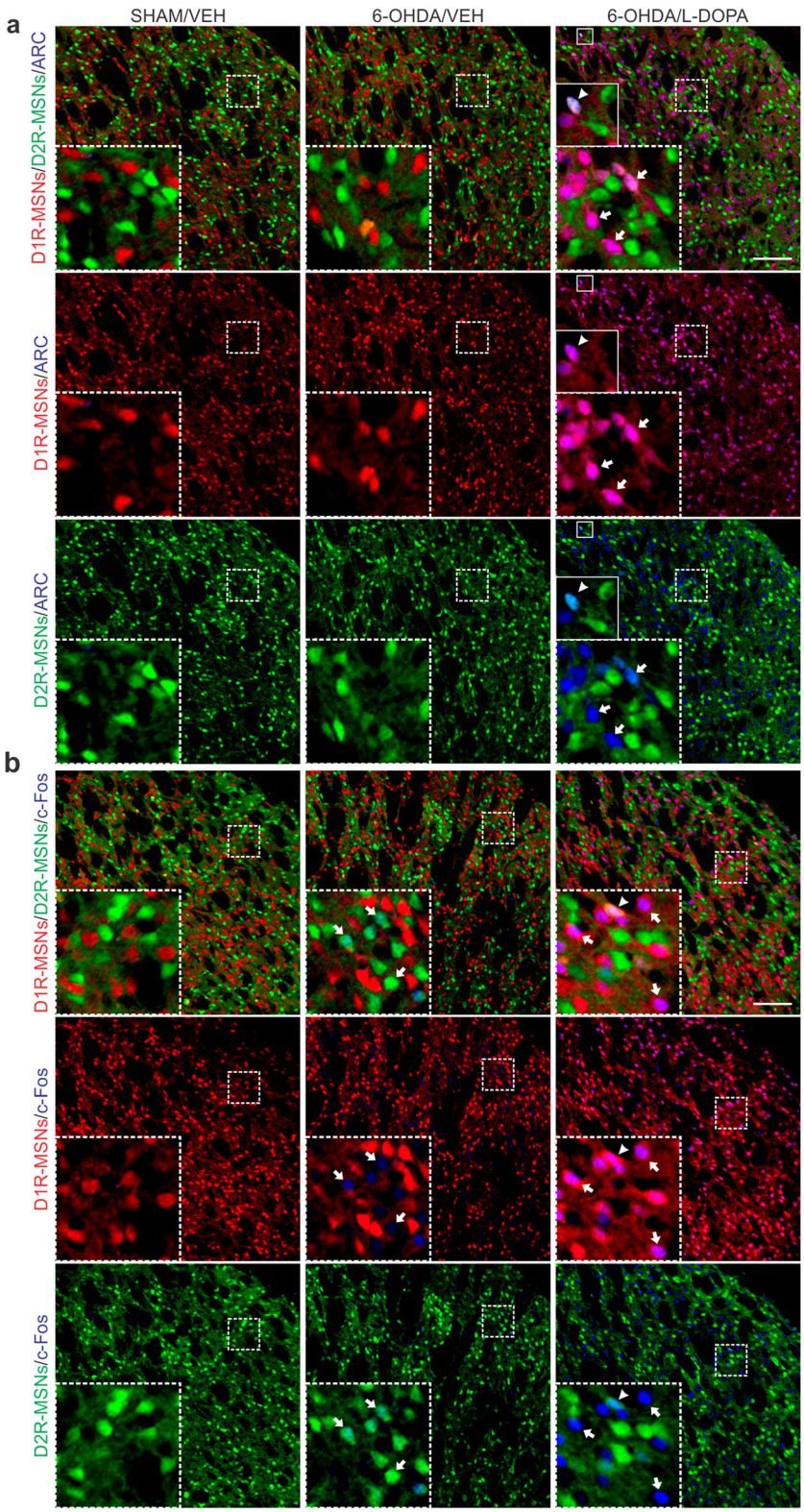

Fig. 4 Representative confocal microphotograph of the dorsolateral striatum of BAC-double transgenic mice showing the autofluorescence of D1R-MSNs (red) and D2R-MSNs (green) and the immunofluorescence of Arc (blue) (**a**) or c-Fos (blue) (**b**). Arrows indicate some D1R-MSNs expressing Arc in the dyskinetic condition (**a**) and some D2R-MSNs or D1R-MSNs expressing c-Fos in lesioned or dyskinetic animals, respectively (**b**). Arrow heads indicate neurons co-expressing both D1 and D2 receptors and Arc (blue) (**a**) or c-Fos (blue) (**b**). The color of Arc and c-Fos fluorescence developed with Cy5 as fluorophore was altered to show them in blue. Scale bars: 100 μm

confirming previous findings [14], using a different lesioning technique of the nigrostriatal pathway.

Similarly, studies analyzing changes in the connections between PV-containing interneurons and MSNs after DA depletion have reached opposite conclusions. One study showed that PV striatal cells doubled their connectivity onto D2R-MSNs; it was proposed that such enhanced inhibitory connectivity would promote neuronal synchrony after DA

Table 1 c-Fos and Arc expression in the different striatal subpopulation of MSNs

		% of Arc or c-Fos immunoreactive MSNs (mean ± SEM)		
	MSNs	SHAM/VEH	6-OHDA/VEH	6-OHDA/L-DOPA
Arc	D1	nd	nd	100 ± 0
	D2	nd	nd	nd
	D1-D2	nd	nd	100 ± 0
c-Fos	D1	nd	1 ± 1	99 ± 1
	D2	nd	51 ± 13	nd
	D1-D2	nd	nd	100 ± 0

Animals per group: SHAM/VEH, $n = 4$; 6-OHDA/VEH, $n = 3$; 6-OHDA/L-DOPA, $n = 4$

depletion [27]. On the contrary, another study showed a reduction in the innervation of both types of MSNs by PV-containing interneurons [28]. We showed that PV-ir contacts onto both types of MSNs are reduced after chronic nigrostriatal lesions. Thus, our findings are closer to those of Salin et al. [28] who studied PV interneurons to MSN connectivity 3 weeks after severe nigrostriatal denervation in rats, than to those of Gittis et al. [27] who used younger mice and studied PV perisomatic boutons less than a week after lesion. Whether LID relates to changes in PV interneurons to MSN connectivity remains unknown, but there is some evidence showing that the pharmacological inhibition of PV interneurons can induce dyskinesia [48]. Here, we found that PV-ir boutons onto both types of MSNs remain pruned after L-DOPA treatment. However, while VGAT-ir contacts are also reduced after DA depletion, they are restored, for D2R-MSNs, or partially restored, for D1R-MSNs, after L-DOPA administration. Thus, L-DOPA therapy seems to restore GABAergic contacts in a PV-independent manner.

The quantification of PV-ir cells showed that striatal PV-ir cell density is reduced after DA depletion. This result is in line with the decreased number of PV-ir boutons observed after 6-OHDA injection. Furthermore, we expected that if the decrease in PV-ir boutons and cell density were due to a decrease in PV expression but not a decrease in FSI number, then there should be an increase in WFA+ cells that do not express PV in 6-OHDA mice. However, DA depletion decreased the number of WFA-labeled cells that do express PV while maintaining the number of WFA-labeled cells that are not PV-ir. These findings suggest that the lower numbers of PV-ir cells and boutons found in lesioned and dyskinetic mice are not due to a decreased expression of PV but to a decreased number of FSI. Remarkably, while L-DOPA did not revert the 6-OHDA lesion–induced decrease in PV-ir cell density, the number of WFA+/PV-ir cells was at intermediate levels between those of SHAM and 6-OHDA groups after L-DOPA treatment, suggesting that a subpopulation of FSI might have lost both PV-ir and the WFA+ net but is still restored by L-DOPA therapy. We speculate that some FSIs are lost after the 6-OHDA lesion while some others have lost PV immunoreactivity and the WFA+ net but can still recover these markers during L-DOPA therapy. In this context, the recovery of VGAT-ir boutons may represent a compensatory increase of a FSI independent perisomatic inhibitory input onto MSNs.

There are many possible explanations for the discrepancy between the number of PV- and VGAT-ir boutons. In addition to PV-ir interneurons, there are other types of interneurons that make GABAergic synapses onto MSNs, including those expressing NPY, somatostatin (SST), and nitric oxide synthase (NOS) [49]. However, while PV-ir synapses are enriched on somata [25] and in proximal dendritic regions [24, 50, 51], SST-ir terminals are enriched on distal dendritic regions [50–52]. Furthermore, GABAergic synaptic connections between D1R- and D2R-MSNs have also been reported. In contrast to the divergent connectivity of FSIs, MSNs appear to show convergent connectivity, so while individual connections are quite weak, an assembly of MSN inputs onto a given MSN is comparable with FSI connections [53]. MSN recurrent collaterals are not randomly distributed: while the majority of their contacts have dendritic location [23], around 12% has somatic location [54]. It follows then that further work is necessary to assess the possibility that these perisomatic GABAergic contacts observed onto MSNs after L-DOPA come from other types of interneurons that have undergone relocalization of their synaptic contacts, like SST/NPY/NOS-ir interneurons, or from other MSNs engaged in lateral inhibition.

Parvalbumin at presynaptic terminals of FSI axons prevents short-term facilitation at the FSI to MSN synapse [55]. It has been reported that the absence of PV in FSI increases short-term facilitation and, therefore, inhibition of MSN [56, 57]. Thus, the reduction of PV and VGAT boutons after the 6-OHDA lesion may reflect a reduction of perisomatic inhibition in this condition, while the selective decrease of PV in the dyskinetic animals with restored levels of VGAT-ir contacts may result in an increased inhibitory effect of the VGAT-positive perisomatic boutons. This decreased inhibition of the MSNs in the 6-OHDA condition might be connected to spine pruning as part of homeostatic mechanisms that tend to

maintain the balance between excitation and inhibition, which is supported by our data showing an overall reduction of both inhibitory and excitatory synaptic connectivity onto both MSN subtypes after a 6-OHDA lesion. The parallel recovery of spine density and perisomatic inhibitory input in D2R-MSNs after L-DOPA treatment could also relate to homeostatic mechanisms trying to maintain the excitatory/inhibitory balance in these cells. On the other hand, D1R-MSNs show a partial recovery of perisomatic inhibitory contacts in the absence of any recovery of spine density, which may still relate to mechanisms counterbalancing excitation, since there is molecular (e.g., c-Fos and Arc overexpression) and functional [58, 59] evidence of exacerbated activity of D1R-MSNs in dyskinetic animals. At the structural level, this enhanced activity may have a correlation with the remodeling of spine morphology reported for D1R-MSNs [14, 15].

The assessment of changes in the expression of immediate-early genes such as c-Fos and Arc is believed to be a useful tool for evaluating neuronal responsiveness to different stimuli [60]. Our data suggest that c-Fos and Arc correlate with different aspects of MSN architecture and function. While the expression pattern of cellular c-Fos seems to correspond well with the changes of activity occurring in MSNs after a nigrostriatal lesion and LID development, Arc expression is limited to D1R-MSNs in LID. D2R-MSNs respond excessively while D1R-MSNs respond less to inputs from motor cortex in vivo after a nigrostriatal lesion [21, 30, 61], which corresponds well with our results showing c-Fos overexpression in the parkinsonian condition only in D2R-MSNs. D2R-MSNs show adaptations that may serve to attenuate, rather than cause, this hyperresponsiveness, such as a decreased input resistance [17] and a reduced density of dendritic spines. A decrease of perisomatic feed-forward inhibition, in contrast, may be causally linked to their hyperresponsiveness to cortical input [21]. On the contrary, spine pruning may be causally related to the D1R-MSN hyporesponsiveness while reduced perisomatic inhibition (and increased input resistance [17]) may help to maintain some degree of activity along the direct pathway. Likewise, c-Fos is highly and selectively expressed in D1R-MSNs 1 h after a L-DOPA challenge inducing dyskinesia, a condition where D1R-MSNs are expected to be hyperactive and D2R-MSNs inhibited [62–64]. These findings are in line with the current belief that these two well-known populations of MSNs expressing either D1 or D2 DA receptors are largely distinct, which, once again, have shown distinct expression patterns and responses to changes in striatal DA levels. However, those MSNs that co-express both types of DA receptors seem to behave more similarly to the D1R-MSNs than the D2R-MSNs, as they expressed c-Fos and Arc only in the dyskinetic condition but not in hemiparkinsonian mice. This is in line with the results of Gagnon et al. [45] that showed that, even though these cells are affected differently than the D1R- and D2R-MSNs by striatal DA deafferentation, they have more in common with the D1R-MSNs than with the D2R-MSNs. As the role and contribution of these neurons to striatal function and dysfunction are still unknown, these novel findings may contribute to better characterize this controversial population of neurons.

Many of the compensatory molecular changes after L-DOPA treatment are selectively observed in D1R-MSNs [65–67]. Among genes associated with synaptic remodeling, Arc was found to be related to LID [68, 69]. Arc mRNA is transported into dendrites after episodes of neuronal activation depending on NMDA receptor activation. Arc protein is assembled into the postsynaptic junction and mediates long-term synapse-specific modifications [70, 71]. Arc expression is highly dynamic and tightly regulated by neuronal activity and experience, and it is required for enduring forms of synaptic plasticity and memory. Our results showed that Arc expression is only observed in D1R-MSNs and only after L-DOPA administration. Arc is not expressed in D2R-MSNs in vehicle-treated 6-OHDA mice although these neurons are hyperactive in this condition [30, 61, 72], nor is it expressed in D2R-MSNs in the LID condition where they show spine regrowth [14, 17]. Thus, Arc selective expression in D1R-MSNs is probably related to some singular aspect of hyperactivity or spine remodeling taking place in these cells in LID. Even though we did not find a restoration of D1R-MSN spine density in LID, it has been previously shown that there is a microstructural remodeling of the remaining spines, which are larger and accompanied by an increase of PSD length [15]. However, synaptic strength remained decreased. On the contrary, the newly formed D2R-MSN spines had shorter PSD length, suggesting that they may not be completely functional [15]. This finding is further supported by our results showing absence of Arc expression in these neurons, as this protein localizes selectively at activated synaptic sites [70].

Taking all this into account, our results suggest that L-DOPA treatment modulates D2R-MSNs in a homeostatic manner, which is highlighted by the opposite changes in c-Fos expression and spine density. This modulation might be responsible for the beneficial effects of L-DOPA, as recent studies show that parkinsonian deficits are not readily detectable in mice until D2R-MSNs become hyperresponsive to cortical input [30] and adult deletion of the D2R is sufficient to produce a marked parkinsonian syndrome in mice [73]. On the contrary, L-DOPA administration in a dose capable of inducing dyskinesia would lead to a new maladaptive scenario, in which D1R-MSNs are pruned of spines but hyperactive as suggested by c-Fos expression, and suffering further spine remodeling, as suggested by Arc expression. This apparent over-activity of the D1 pathway is in line with

the current belief that emphasizes the role of D1R as a main player in the induction of LID.

Acknowledgements The authors would like to thank Germán La Iacona for his technical assistance.

Funding Information This work was supported by grants from the Argentine Agency for the Promotion of Science (PICT 2011-1758 and PICT 2015-3687), University of Buenos Aires (UBACyT 2014-2017 249), and Argentine National Research Council (CONICET, PIP 2013-0401) and by grants from the Spanish Ministries of Economía, Industria y Competitividad (SAF2016-78207-R) and PCIN-2015-098 and of Sanidad Servicios Sociales e Igualdad (ISCIII, CIBERNED CB06/05/0055, PNSD2016I033) and 172275 from Ramón Areces Foundation to RM. GG is a research fellow of the CONICET. LR, JEB, MGM, and IRET are members of the research career of CONICET.

Compliance with Ethical Standards

All surgical procedures and experimental manipulations were performed in accordance with European Council Directive 2010/63/EU guidelines for the care of laboratory animals and the regulations for the Care and Use of Laboratory Animals of the National Institutes of Health, USA. Animal experiments were approved by our local Ethics Committee (IACUC EXP-UBA No. 0027665/2014).

Conflict of Interest The authors declare that they have no competing interests.

Publisher's Note Springer Nature remains neutral with regard to jurisdictional claims in published maps and institutional affiliations.

References

1. Birkmayer W, Hornykiewicz O (1961) The L-3,4-dioxyphenylalanine (DOPA)-effect in Parkinson-akinesia. Wien Klin Wochenschr 73:787–788
2. Cramer SC, Sur M, Dobkin BH, O'Brien C, Sanger TD, Trojanowski JQ, Rumsey JM, Hicks R et al (2011) Harnessing neuroplasticity for clinical applications. Brain 134:1591–1609. https://doi.org/10.1093/brain/awr039
3. Holtmaat A, Caroni P (2016) Functional and structural underpinnings of neuronal assembly formation in learning. Nat Neurosci 19:1553–1562. https://doi.org/10.1038/nn.4418
4. Butz M, Wörgötter F, van Ooyen A (2009) Activity-dependent structural plasticity. Brain Res Rev 60:287–305. https://doi.org/10.1016/j.brainresrev.2008.12.023
5. Graf ER, Zhang X, Jin S-X, Linhoff MW, Craig AM (2004) Neurexins induce differentiation of GABA and glutamate postsynaptic specializations via neuroligins. Cell 119:1013–1026. https://doi.org/10.1016/j.cell.2004.11.035
6. Liu G (2004) Local structural balance and functional interaction of excitatory and inhibitory synapses in hippocampal dendrites. Nat Neurosci 7:373–379. https://doi.org/10.1038/nn1206
7. Prange O, Wong TP, Gerrow K, Wang YT, el-Husseini A (2004) A balance between excitatory and inhibitory synapses is controlled by PSD-95 and neuroligin. Proc Natl Acad Sci 101:13915–13920. https://doi.org/10.1073/pnas.0405939101
8. Levinson JN, El-Husseini A (2005) Building excitatory and inhibitory synapses: balancing neuroligin partnerships. Neuron 48:171–174. https://doi.org/10.1016/j.neuron.2005.09.017
9. Kawaguchi Y (1997) Neostriatal cell subtypes and their functional roles. Neurosci Res 27:1–8
10. Bolam J, Hanley J, Booth P, Bevan M (2000) Synaptic organisation of the basal ganglia. J Anat 196:527–542. https://doi.org/10.1046/j.1469-7580.2000.19640527.x
11. Gerfen CR, Young WS (1988) Distribution of striatonigral and striatopallidal peptidergic neurons in both patch and matrix compartments: an in situ hybridization histochemistry and fluorescent retrograde tracing study. Brain Res 460:161–167
12. Gerfen CR, Surmeier DJ (2011) Modulation of striatal projection systems by dopamine. Annu Rev Neurosci 34:441–466. https://doi.org/10.1146/annurev-neuro-061010-113641
13. Chen Y, Sabatini BL (2012) Signaling in dendritic spines and spine microdomains. Curr Opin Neurobiol 22:389–396. https://doi.org/10.1016/j.conb.2012.03.003
14. Suárez L, Solís O, Caramés J et al (2014) L-DOPA treatment selectively restores spine density in dopamine receptor d2-expressing projection neurons in dyskinetic mice. Biol Psychiatry 75:711–722. https://doi.org/10.1016/j.biopsych.2013.05.006
15. Suarez LM, Solis O, Aguado C, Lujan R, Moratalla R (2016) L-DOPA oppositely regulates synaptic strength and spine morphology in D1 and D2 striatal projection neurons in dyskinesia. Cereb Cortex 26:4253–4264. https://doi.org/10.1093/cercor/bhw263
16. Nishijima H, Suzuki S, Kon T, Funamizu Y, Ueno T, Haga R, Suzuki C, Arai A et al (2014) Morphologic changes of dendritic spines of striatal neurons in the levodopa-induced dyskinesia model. Mov Disord 29:336–343. https://doi.org/10.1002/mds.25826
17. Fieblinger T, Graves SM, Sebel LE, Alcacer C, Plotkin JL, Gertler TS, Chan CS, Heiman M et al (2014) Cell type-specific plasticity of striatal projection neurons in parkinsonism and L-DOPA-induced dyskinesia. Nat Commun 5:5316. https://doi.org/10.1038/ncomms6316
18. Zhang Y, Meredith GE, Mendoza-Elias N, Rademacher DJ, Tseng KY, Steece-Collier K (2013) Aberrant restoration of spines and their synapses in L-DOPA-induced dyskinesia: involvement of corticostriatal but not thalamostriatal synapses. J Neurosci 33:11655–11667. https://doi.org/10.1523/JNEUROSCI.0288-13.2013
19. Kawaguchi Y (1993) Physiological, morphological, and histochemical characterization of three classes of interneurons in rat neostriatum. J Neurosci 13:4908–4923
20. Tepper JM, Tecuapetla F, Koós T, Ibáñez-Sandoval O (2010) Heterogeneity and diversity of striatal GABAergic interneurons. Front Neuroanat 4:150. https://doi.org/10.3389/fnana.2010.00150
21. Mallet N, Ballion B, Le Moine C, Gonon F (2006) Cortical inputs and GABA interneurons imbalance projection neurons in the striatum of parkinsonian rats. J Neurosci 26:3875–3884. https://doi.org/10.1523/JNEUROSCI.4439-05.2006
22. Berke JD, Okatan M, Skurski J, Eichenbaum HB (2004) Oscillatory entrainment of striatal neurons in freely moving rats. Neuron 43:883–896. https://doi.org/10.1016/j.neuron.2004.08.035
23. Tepper JM, Koós T, Wilson CJ (2004) GABAergic microcircuits in the neostriatum. Trends Neurosci 27:662–669. https://doi.org/10.1016/j.tins.2004.08.007
24. Kita H, Kosaka T, Heizmann CW (1990) Parvalbumin-immunoreactive neurons in the rat neostriatum: a light and electron microscopic study. Brain Res 536:1–15
25. Bennett B, Bolam J (1994) Synaptic input and output of parvalbumin-immunoreactive neurons in the neostriatum of the rat. Neuroscience 62:707–719
26. Gittis AH, Nelson AB, Thwin MT, Palop JJ, Kreitzer AC (2010) Distinct roles of GABAergic interneurons in the regulation of striatal output pathways. J Neurosci 30:2223–2234. https://doi.org/10.1523/JNEUROSCI.4870-09.2010
27. Gittis AH, Hang GB, LaDow ES et al (2011) Rapid target-specific remodeling of fast-spiking inhibitory circuits after loss of

dopamine. Neuron 71:858–868. https://doi.org/10.1016/j.neuron.2011.06.035
28. Salin P, López IP, Kachidian P, Barroso-Chinea P, Rico AJ, Gómez-Bautista V, Coulon P, Kerkerian-le Goff L et al (2009) Changes to interneuron-driven striatal microcircuits in a rat model of Parkinson's disease. Neurobiol Dis 34:545–552. https://doi.org/10.1016/j.nbd.2009.03.006
29. Shuen J, Chen M, Gloss B, Calakos N (2008) Drd1a-tdTomato BAC transgenic mice for simultaneous visualization of medium spiny neurons in the direct and indirect pathways of the basal ganglia. J Neurosci 28:2681–2685. https://doi.org/10.1523/JNEUROSCI.5492-07.2008
30. Escande MV, Taravini IRE, Zold CL, Belforte JE, Murer MG (2016) Loss of homeostasis in the direct pathway in a mouse model of asymptomatic parkinson's disease. J Neurosci 36:5686–5698. https://doi.org/10.1523/JNEUROSCI.0492-15.2016
31. Paxinos G, Franklin KBJ (2001) The mouse brain in stereotaxic coordinates, 2nd edn. Academic Press, San Diego
32. Cenci MA, Lundblad M (2007) Ratings of L-DOPA-induced dyskinesia in the unilateral 6-OHDA lesion model of Parkinson's disease in rats and mice. Curr Protoc Neurosci Chapter 9:Unit 9.25. https://doi.org/10.1002/0471142301.ns0925s41
33. Francardo V, Recchia A, Popovic N, Andersson D, Nissbrandt H, Cenci MA (2011) Impact of the lesion procedure on the profiles of motor impairment and molecular responsiveness to L-DOPA in the 6-hydroxydopamine mouse model of Parkinson's disease. Neurobiol Dis 42:327–340. https://doi.org/10.1016/j.nbd.2011.01.024
34. Espadas I, Darmopil S, Vergaño-Vera E, Ortiz O, Oliva I, Vicario-Abejón C, Martín ED, Moratalla R (2012) L-DOPA-induced increase in TH-immunoreactive striatal neurons in parkinsonian mice: insights into regulation and function. Neurobiol Dis 48:271–281. https://doi.org/10.1016/j.nbd.2012.07.012
35. Larramendy C, Taravini IRE, Saborido MD, Ferrario JE, Murer MG, Gershanik OS (2008) Cabergoline and pramipexole fail to modify already established dyskinesias in an animal model of parkinsonism. Behav Brain Res 194:44–51. https://doi.org/10.1016/j.bbr.2008.06.021
36. Lundblad M, Picconi B, Lindgren H, Cenci MA (2004) A model of L-DOPA-induced dyskinesia in 6-hydroxydopamine lesioned mice: relation to motor and cellular parameters of nigrostriatal function. Neurobiol Dis 16:110–123. https://doi.org/10.1016/j.nbd.2004.01.007
37. Ruiz-Dediego I, Mellstrom B, Vallejo M et al (2015) Activation of DREAM (downstream regulatory element antagonistic modulator), a calcium-binding protein, reduces L-DOPA-induced dyskinesias in mice. Biol Psychiatry 77:95–105. https://doi.org/10.1016/j.biopsych.2014.03.023
38. Solís O, Garcia-Montes JR, González-Granillo A, Xu M, Moratalla R (2017) Dopamine D3 receptor modulates L-DOPA-induced dyskinesia by targeting D1 receptor-mediated striatal signaling. Cereb Cortex 27:435–446. https://doi.org/10.1093/cercor/bhv231
39. Taravini IRE, Ferrario JE, Delbe J, Ginestet L, Debeir T, Courty J, Murer MG, Gershanik OS et al (2005) Immunodetection of heparin-binding growth associated molecule (pleiotrophin) in striatal interneurons. Brain Res 1066:196–200. https://doi.org/10.1016/j.brainres.2005.10.055
40. Taravini IRE, Chertoff M, Cafferata EG, Courty J, Murer MG, Pitossi FJ, Gershanik OS (2011) Pleiotrophin over-expression provides trophic support to dopaminergic neurons in parkinsonian rats. Mol Neurodegener 6:40. https://doi.org/10.1186/1750-1326-6-40
41. Elston GN, Benavides-Piccione R, DeFelipe J (2001) The pyramidal cell in cognition: a comparative study in human and monkey. J Neurosci 21:RC163
42. Enwright JF, Sanapala S, Foglio A et al (2016) Reduced labeling of parvalbumin neurons and perineuronal nets in the dorsolateral prefrontal cortex of subjects with schizophrenia. Neuropsychopharmacology 41:2206–2214. https://doi.org/10.1038/npp.2016.24
43. Braz BY, Galiñanes GL, Taravini IR et al (2015) Altered corticostriatal connectivity and exploration/exploitation imbalance emerge as intermediate phenotypes for a neonatal dopamine dysfunction. Neuropsychopharmacology 40:1–12. https://doi.org/10.1038/npp.2015.104
44. Sholl DA (1953) Dendritic organization in the neurons of the visual and motor cortices of the cat. J Anat 87:387–406
45. Gagnon D, Petryszyn S, Sanchez MG, Bories C, Beaulieu JM, de Koninck Y, Parent A, Parent M (2017) Striatal neurons expressing D1 and D2 receptors are morphologically distinct and differently affected by dopamine denervation in mice. Sci Rep 7:9–17. https://doi.org/10.1038/srep41432
46. McNeill TH, Brown SA, Rafols JA, Shoulson I (1988) Atrophy of medium spiny I striatal dendrites in advanced Parkinson's disease. Brain Res 455:148–152
47. Zaja-Milatovic S, Milatovic D, Schantz AM, Zhang J, Montine KS, Samii A, Deutch AY, Montine TJ (2005) Dendritic degeneration in neostriatal medium spiny neurons in Parkinson disease. Neurology 64:545–547. https://doi.org/10.1212/01.WNL.0000150591.33787.A4
48. Gittis AH, Leventhal DK, Fensterheim B et al (2011) Selective inhibition of striatal fast-spiking interneurons causes dyskinesias. J Neurosci 31:15727–15731. https://doi.org/10.1523/JNEUROSCI.3875-11.2011
49. Galarraga E, Vilchis C, Tkatch T, Salgado H, Tecuapetla F, Perez-Rosello T, Perez-Garci E, Hernandez-Echeagaray E et al (2007) Somatostatinergic modulation of firing pattern and calcium-activated potassium currents in medium spiny neostriatal neurons. Neuroscience 146:537–554. https://doi.org/10.1016/j.neuroscience.2007.01.032
50. Kubota Y, Kawaguchi Y (2000) Dependence of GABAergic synaptic areas on the interneuron type and target size. J Neurosci 20:375–386
51. Straub C, Saulnier JL, Bègue A, Feng DD, Huang KW, Sabatini BL (2016) Principles of synaptic organization of GABAergic interneurons in the striatum. Neuron 92:84–92. https://doi.org/10.1016/j.neuron.2016.09.007
52. DiFiglia M, Aronin N (1982) Ultrastructural features of immunoreactive somatostatin neurons in the rat caudate nucleus. J Neurosci 2:1267–1274
53. Chuhma N, Tanaka KF, Hen R, Rayport S (2011) Functional connectome of the striatal medium spiny neuron. J Neurosci 31:1183–1192. https://doi.org/10.1523/JNEUROSCI.3833-10.2011
54. Wilson CJ, Groves PM (1980) Fine structure and synaptic connections of the common spiny neuron of the rat neostriatum: a study employing intracellular inject of horseradish peroxidase. J Comp Neurol 194:599–615. https://doi.org/10.1002/cne.901940308
55. Caillard O, Moreno H, Schwaller B, Llano I, Celio MR, Marty A (2000) Role of the calcium-binding protein parvalbumin in short-term synaptic plasticity. Proc Natl Acad Sci U S A 97:13372–13377. https://doi.org/10.1073/pnas.230362997
56. Orduz D, Bischop DP, Schwaller B, Schiffmann SN, Gall D (2013) Parvalbumin tunes spike-timing and efferent short-term plasticity in striatal fast spiking interneurons. J Physiol 591:3215–3232. https://doi.org/10.1113/jphysiol.2012.250795
57. Filice F, Vörckel KJ, Sungur AÖ, Wöhr M, Schwaller B (2016) Reduction in parvalbumin expression not loss of the parvalbumin-expressing GABA interneuron subpopulation in genetic parvalbumin and shank mouse models of autism. Mol Brain 9:10. https://doi.org/10.1186/s13041-016-0192-8
58. Parker JG, Marshall JD, Ahanonu B, Wu YW, Kim TH, Grewe BF, Zhang Y, Li JZ et al (2018) Diametric neural ensemble dynamics in

parkinsonian and dyskinetic states. Nature 557:177–182. https://doi.org/10.1038/s41586-018-0090-6
59. Girasole AE, Lum MY, Nathaniel D, Bair-Marshall CJ, Guenthner CJ, Luo L, Kreitzer AC, Nelson AB (2018) A subpopulation of striatal neurons mediates levodopa-induced dyskinesia. Neuron 97:787–795.e6. https://doi.org/10.1016/j.neuron.2018.01.017
60. Wang JQ, Smith AJ, McGinty JF (1995) A single injection of amphetamine or methamphetamine induces dynamic alterations in c-fos, zif/268 and preprodynorphin messenger RNA expression in rat forebrain. Neuroscience 68:83–95
61. Kravitz AV, Freeze BS, Parker PRL et al (2010) Regulation of parkinsonian motor behaviors by optogenetic control of basal ganglia circuitry. Nature 466:622–626. https://doi.org/10.1038/nature09159.Regulation
62. Aubert I, Guigoni C, Håkansson K, Li Q, Dovero S, Barthe N, Bioulac BH, Gross CE et al (2005) Increased D1 dopamine receptor signaling in levodopa-induced dyskinesia. Ann Neurol 57:17–26. https://doi.org/10.1002/ana.20296
63. Picconi B, Centonze D, Håkansson K, Bernardi G, Greengard P, Fisone G, Cenci MA, Calabresi P (2003) Loss of bidirectional striatal synaptic plasticity in L-DOPA–induced dyskinesia. Nat Neurosci 6:501–506. https://doi.org/10.1038/nn1040
64. Picconi B, Paillé V, Ghiglieri V, Bagetta V, Barone I, Lindgren HS, Bernardi G, Angela Cenci M et al (2008) l-DOPA dosage is critically involved in dyskinesia via loss of synaptic depotentiation. Neurobiol Dis 29:327–335. https://doi.org/10.1016/j.nbd.2007.10.001
65. Andersson M, Hilbertson A, Cenci MA (1999) Striatal fosB expression is causally linked with l-DOPA-induced abnormal involuntary movements and the associated upregulation of striatal prodynorphin mRNA in a rat model of Parkinson's disease. Neurobiol Dis 6:461–474. https://doi.org/10.1006/nbdi.1999.0259S0969-9961(99)90259-0
66. Feyder M, Bonito-Oliva A, Fisone G (2011) L-DOPA-induced dyskinesia and abnormal signaling in striatal medium spiny neurons: focus on dopamine D1 receptor-mediated transmission. Front Behav Neurosci 5:71. https://doi.org/10.3389/fnbeh.2011.00071
67. Westin JE, Vercammen L, Strome EM, Konradi C, Cenci MA (2007) Spatiotemporal pattern of striatal ERK1/2 phosphorylation in a rat model of L-DOPA-induced dyskinesia and the role of dopamine D1 receptors. Biol Psychiatry 62:800–810. https://doi.org/10.1016/j.biopsych.2006.11.032
68. Sgambato-Faure V, Buggia V, Gilbert F, Lévesque D, Benabid AL, Berger F (2005) Coordinated and spatial upregulation of arc in striatonigral neurons correlates with L-dopa-induced behavioral sensitization in dyskinetic rats. J Neuropathol Exp Neurol 64:936–947. https://doi.org/10.1097/01.jnen.0000186922.42592.b7
69. Bastide MF, Dovero S, Charron G, Porras G, Gross CE, Fernagut PO, Bézard E (2014) Immediate-early gene expression in structures outside the basal ganglia is associated to l-DOPA-induced dyskinesia. Neurobiol Dis 62:179–192. https://doi.org/10.1016/j.nbd.2013.09.020
70. Steward O, Wallace CS, Lyford GL, Worley PF (1998) Synaptic activation causes the mRNA for the IEG Arc to localize selectively near activated postsynaptic sites on dendrites. Neuron 21:741–751
71. Steward O, Worley P (2002) Local synthesis of proteins at synaptic sites on dendrites: role in synaptic plasticity and memory consolidation? Neurobiol Learn Mem 78:508–527
72. Shen W, Flajolet M, Greengard P, Surmeier DJ (2008) Dichotomous dopaminergic control of striatal synaptic plasticity. Science 321:848–851. https://doi.org/10.1126/science.1160575
73. Bello EP, Casas-Cordero R, Galiñanes GL, Casey E, Belluscio MA, Rodríguez V, Noaín D, Murer MG et al (2017) Inducible ablation of dopamine D2 receptors in adult mice impairs locomotion, motor skill learning and leads to severe parkinsonism. Mol Psychiatry 22:595–604. https://doi.org/10.1038/mp.2016.105